Geological Magazine

www.cambridge.org/geo

Frasnian (Upper Devonian) integrated facies analysis, magnetic susceptibility and sea-level fluctuations in the NW Algerian Sahara

Abdessamed Mahboubi[1], Jean-Jacques Cornée[2], Raimund Feist[1], Pierre Camps[2] and Catherine Girard[1]

[1]Institut des Sciences de l'Evolution, Université de Montpellier, CNRS, IRD, CC064, Place Eugène Bataillon, Montpellier Cedex 05, France and [2]Géosciences Montpellier, CNRS, Université de Montpellier, Université des Antilles, France

Original Article

Cite this article: Mahboubi A, Cornée J-J, Feist R, Camps P, and Girard C (2019) Frasnian (Upper Devonian) integrated facies analysis, magnetic susceptibility and sea-level fluctuations in the NW Algerian Sahara. *Geological Magazine* **156**: 1295–1310. https://doi.org/10.1017/S0016756818000626

Received: 22 August 2017
Revised: 19 July 2018
Accepted: 2 August 2018
First published online: 18 October 2018

Keywords:
Frasnian; Algerian Sahara; facies; magnetic susceptibility; sea level

Author for correspondence:
Jean-Jacques Cornée, Email: jean-jacques.cornee@gm.univ-montp2.fr

Abstract

Changes in the palaeoenvironment are investigated in two representative Frasnian sections of the NW Algerian Sahara, integrating sedimentology and magnetic susceptibility (MS). The Ben Zireg section is characterized by condensed and ferruginous calcareous deposits; in the South Marhouma section the sedimentation rate is high, dominated by muddy nodular limestones with several hypoxic shale intervals. In both sections, sediments were mostly emplaced on pelagic outer ramps below the limit of storm wave-base, evolving through time from proximal to distal setting. Investigations of the temporal evolution of facies and MS data permit a first estimate of the local sea-level trends in NW Algeria. These trends match the overall long-term rise of sea level recognized worldwide from Frasnian Zone 5 upwards. Noteable positive excursions of the sea-level curve related to the *semichatovae* transgression, as well as to the late Frasnian transgression prior to the late Kellwasser event, can be established in this area. Although the sharp regression of sea level at the upper Kellwasser level can be confirmed from our data, no particular trend is depicted at the transition of conodont zones (Frasnian Zones 12–13) where the presence of the lower Kellwasser level has not yet been clearly recognized.

1. Introduction

The Frasnian Stage (Upper Devonian) is remarkable in that it preserved one of the major Palaeozoic sea-level rises (Haq & Shutter, 2008; Morrow & Sandberg, 2008), which culminated in the spreading of basinal anoxic waters. Major biotic turnovers occurred during the early and late Kellwasser Events during latest Frasnian time (e.g. Hallam & Wignall, 1999), which was also a period of origination of new faunas (Bambach *et al.* 2004; Stigall, 2012). This long-term eustatic rise was documented mainly in Laurussia (e.g. Johnson *et al.* 1985; Johnson & Sandberg, 1988; Narkiewicz, 1988; Alekseev *et al.* 1996; House & Ziegler, 1997; Filer, 2002; Bond & Wignall, 2008; Morrow & Sandberg, 2008) and in South China (Chen & Tucker, 2003). Using preliminary records from the Moroccan Anti-Atlas (Wendt & Belka, 1991), one accurate sea-level curve was recently provided on the African Gondwana margin (Dopieralska *et al.* 2016).

In this contribution we focus on Upper Devonian facies and sea-level fluctuations in the Algerian Sahara by integrating results from two representative Frasnian sections of different marine palaeoenvironmental settings: the South Marhouma (MH) and the Ben Zireg (BZ) sections (Fig. 1a). Indeed, this area is still poorly understood compared with the time-equivalent North America and European regions.

Analyses of lithofacies, magnetic susceptibility (MS) and conodont biofacies were performed to determine changes in the depositional environment and sea level through time. MS data record the changes in the amount of detrital content in rocks that may potentially be related to sea-level variations (e.g. Crick *et al.* 2001). The MS signal can be obscured by sedimentary processes and diagenesis, and should be tested by additional magnetic techniques (Da Silva *et al.* 2009, 2013). Conodont genera are often thought to be associated with typical water depth preferences during Late Devonian time. The proportions of each genus within a level were therefore interpreted as a proxy for water depth variation, an approach known as conodont biofacies (Seddon & Sweet, 1971; Sandberg, 1976). However, we are aware that changes in bathymetry might not be the only cause of fluctuations in the percentage of conodont genera in succeeding populations (Belka & Wendt, 1992; Vierek & Racki, 2011). At least four genera (*Polygnathus*, *Icriodus*, *Ancyrodella* and *Palmatolepis*) were present during early–late Frasnian time, and can provide information about depositional environments.

The main objectives of this study are first to determine whether observed changes and trends in the environment occur concomitantly in different settings of the region and, second, to propose a second-order relative sea-level curve through the Frasnian Age that can be compared with

© Cambridge University Press 2018.

CAMBRIDGE UNIVERSITY PRESS

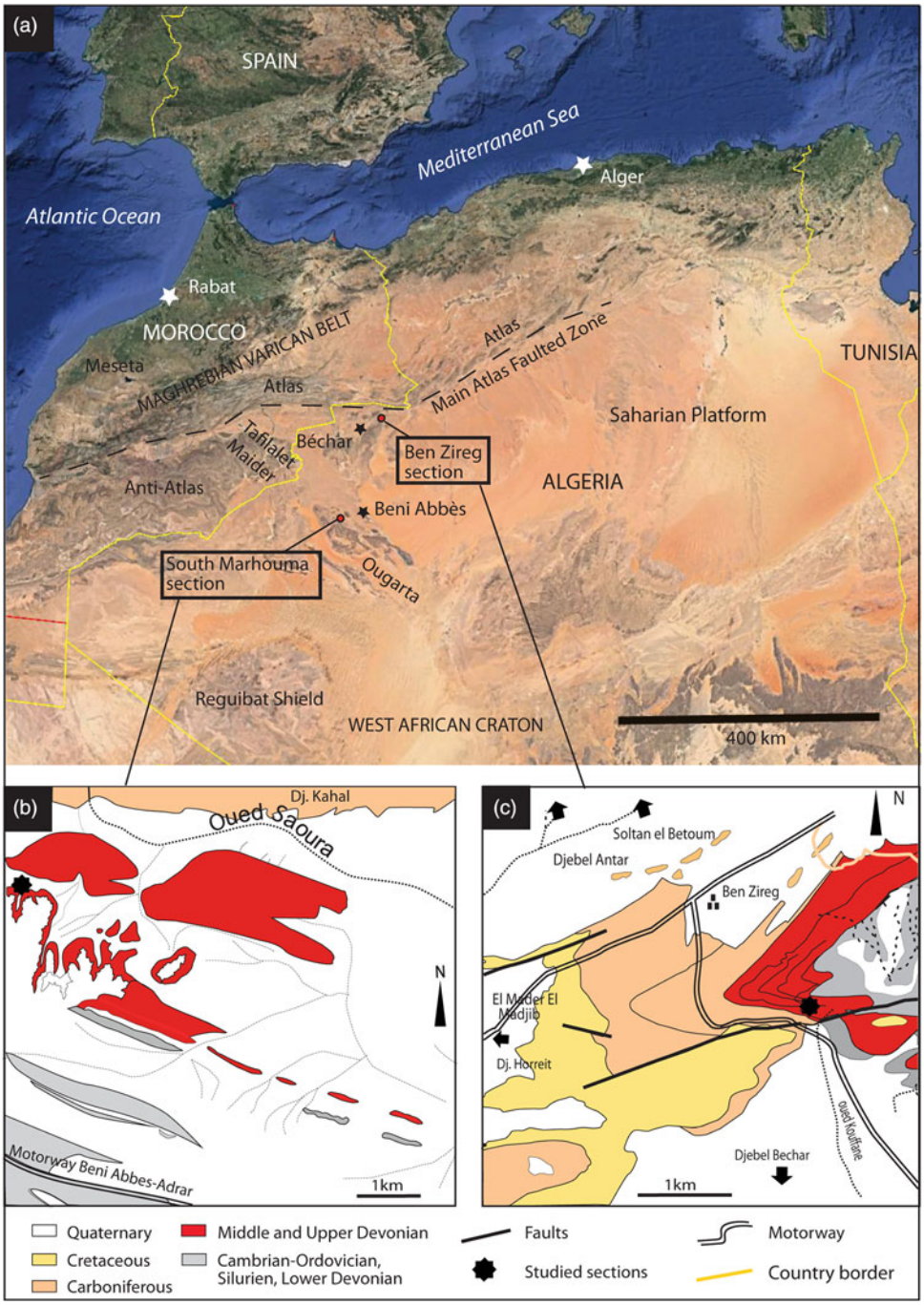

Fig. 1. (Colour online) (**a**) Location of South Marhouma section (Ougarta Basin) and Ben Zireg section (Bechar Basin) in NW Algeria (photograph from Google Earth). (**b**) Investigated section in the Saoura region (after Petter, 1959). (**c**) Investigated section in the Ben Zireg anticline (after Pareyn, 1961).

data from other continental entities. As such, we aim to compare fluctuations in sea level with those determined in the neighbouring Tafilalt region by analysing the Nd isotope composition of conodonts (ε_{Nd} decrease during regressions and increase during transgressions; Dopieralska *et al.* 2016) and with the global trends in Laurussia by using sedimentological data.

2. Geological setting

The Algerian Sahara is part of the North Gondwana epicontinental margin between the Maghrebian Variscan Belt to the north and the West African Craton to the south (Fig. 1a). This domain was moderately affected by the Variscan deformation. The South Marhouma section is located in the intracratonic Ougarta Basin that is bordered to the south by a Precambrian shield. This basin was a strongly subsiding trough filled with continental and marine Ordovician–Carboniferous sediments, up to 10 km in thickness and slightly deformed by Variscan compressional movements (Donzeau, 1974). Upper Devonian deposits are well exposed in the northern part of the basin. At least 75 m of Frasnian sediments continuously crop out in the South Marhouma section (29° 57′ 31.6′′ N, 002° 06′ 07.8′′ W; Fig. 1b). The succession comprises mudrock deposits (shales and marls) containing argillaceous micritic nodules and, at its top, black shales that correspond to the upper Kellwasser horizon (Mahboubi *et al.* 2015). Goniatites from this area were described by Petter (1952) and Göddertz

https://doi.org/10.1017/S0016756818000626 Published online by Cambridge University Press

(1987) and trilobites by Feist *et al.* (2016), and ichnological analyses were performed by Bendella & Mehadji (2014). The first conodont research was conducted by Mahboubi & Gatovsky (2014) and revealed a rather moderate yield of often insignificant conodont elements (less than 10 conodonts per kilogram in most samples), preventing a fine-scaled biostratigraphic framework from being established. However, the presence of a restricted number of conodont zones, that is, Frasnian Zones (FZ) 5, 11, 12 and 13 (Klapper & Kirchgasser, 2016), were recognized with confidence, whereas zones 6 and 7 and 8–10 remain undifferentiated. Many dark shale intervals, notably at the base of the succession (FZ1–4?) and in the uppermost part, did not provide any conodonts. At present, we rely on these poor data that only permit an incomplete zonation to be established at South Marhouma.

In contrast to the high sedimentation rates in the Ougarta trough, sedimentation rates were much lower in the Bechar region some 300 km further to the north. Here, Upper Devonian deposits represent condensed carbonate successions punctuated by hiatuses (Weyant, 1988). The Frasnian succession is most complete in the Ben Zireg section (31° 54′ 39.4′′ N, 001° 47′ 58.8′′ W; Fig. 1c) on the steep southern flank of an acute anticlinal structure. Conodont-based biostratigraphy revealed an upper Givetian – lower Frasnian hiatus, superseded by a complete sequence where all conodont zones from FZ5 to the top of FZ13, corresponding to the Frasnian–Famennian boundary, were recognized (Mahboubi *et al.* 2015). At the top of the succession a marker bed of typical Kellwasser facies is developed.

3. Materials and methods

Samples of well-cemented rock were collected in intervals ranging from 0.2 m to 2 m, depending on the thickness of the soft shale intercalations. A total of 40 and 60 thin-sections were prepared from rock samples from the South Marhouma and Ben Zireg sections, respectively, in order to analyse petrofacies and fabrics. Microfacies descriptions follow Dunham (1962) for carbonate rocks and Schieber (1989) for black shales. The identified facies were interpreted and related to a depositional setting according to Wright & Burchette (1996), Flügel (2004) and Pas *et al.* (2013, 2014). Photographs were taken with an integrated Olympus digital camera. The uppermost Frasnian shales were also studied using the tungsten-filament JEOL 5600 scanning electron microscope (SEM) of the Department of Electron Microscopy and Analytics (MEA) of the University of Montpellier. The resolution of this SEM is of the order of a few microns.

MS measurements were performed on 90 and 54 samples from the South Marhouma and Ben Zireg sections, respectively, for preliminary investigation. Various lithologies were measured (shales and arenaceous and carbonate rocks). In the laboratory, samples were cleaned from iron coatings prior to weighing with a highly accurate balance (with a precision of 0.01 g). MS was measured on samples weighing 5–10 g with a Bartington susceptibility meter (MS-2), which provided measurements in units of $\times 10^{-8}$ m^3 kg^{-1}.

4. Results

4.a. Lithostratigraphy

Each section in the field was first described on the basis of informal lithostratigraphic units, that is, stratified bodies of rocks defined and characterized on the basis of their lithologic properties and ages.

4.a.1. Ben Zireg section

The Ben Zireg section is 26.6 m thick (Fig. 2) and includes five units (Units 1–5) extending from the middle Frasnian to the lower Famennian strata (Mahboubi *et al.* 2015). The succession is dominated by rhythmic, fine-grained carbonates.

Unit 1 contains conodonts representative of FZ5 *(Palmatolepis punctata)* just above a depositional hiatus of early Frasnian age. This unit is characterized by ochre, sometimes brecciated, cherty beds with convolute lamination (Fig. 3a). Thin iron hydroxide coatings are displayed at the top of the unit.

Unit 2 contains conodonts representative of FZ6 (*Ancyrodella gigas* form 2). It consists of greyish to brownish massive limestone beds, of centimetre to decimetre thickness, intercalated by millimetre- to centimetre-thick argillaceous limestone beds that display discrete nodular structures (Fig. 3b).

Unit 3 contains conodonts representative of the interval ranging from FZ7 (*An. lobata* and *An. curvata*) to FZ11 (*Pa. feisti*). It is characterized by well-bedded lime and argillaceous mudstone to wackestone. Beds are frequently coated at the top by iron hydroxide films. The limestone beds are often wackestone with abundant pelagic microfauna (tentaculites and entomozoan crustaceans) associated with sparse euhedral pyrites and some phosphate grains. The amount of nodular structures increases progressively upwards and they are mostly related to pressure-dissolution surfaces.

Unit 4 contains conodonts representative of FZ12 (*Pa. winchelli*), and is characterized by yellowish, massive, clay-rich limestones sometimes interbedded with thin dark shales. Clay-rich limestones display poorly defined nodules (pseudo-nodular limestones). The limestones are mudstone to wackestone with sparse pelagic bioclasts (Fig. 2), some of which are slightly bioturbated.

Unit 5 extends from FZ13 (*Pa. bogartensis)* to the lower Famennian strata (*Pa. triangularis*). It consists of greyish and pinkish nodular to pseudo-nodular limestones and interbedded argillaceous micrite yielding rare faunas, including tentaculite and cephalopod fragments. A 30-cm-thick interval of laminated dark grey to black shales, overlain by 35-cm-thick laminated pinkish fine-grained lime wackestone ('calcisiltites') without fossils (Fig. 3c), is observed in the upper part of the limestones. The dark shales represent the upper Kellwasser horizon.

4.a.2. South Marhouma section

The Frasnian succession is approximately 75 m thick and includes four units (Units 1–4). The base of this section cannot be precisely dated because of a lack of conodont specimens. Details concerning conodont contents and their biostratigraphic implications were presented in Mahboubi & Gatovsky (2014). In contrast to Ben Zireg, this section is dominated by monotonous shale deposits rich in carbonate nodules (Fig. 4).

Unit 1 contains conodonts (*Ancyrodella* sp.) attributed to the FZ1–4 interval as FZ5 was identified in Unit 2. It consists of dark grey shales (Fig. 3d) with some nodular limestones and some black shale interbeds.

Unit 2 extends from FZ5 (*Pa. punctata*) to the lower part of the undifferentiated FZ8–10 interval (*Ancyrognathus coeni* – *Ancyrodella lobata*). It is characterized by centimetre- to decimetre-thick, greyish to reddish, pseudo-nodular to nodular bioclastic limestones (Fig. 3e), which alternate with unfossiliferous greyish to blackish shales. The limestones are wackestones with *Styliolina* (tentaculites) coquinas; they yield phacopid trilobites and cephalopods (*Mesobeloceras* sp.) on the surface of bed MH9 (Feist *et al.* 2016).

https://doi.org/10.1017/S0016756818000626 Published online by Cambridge University Press

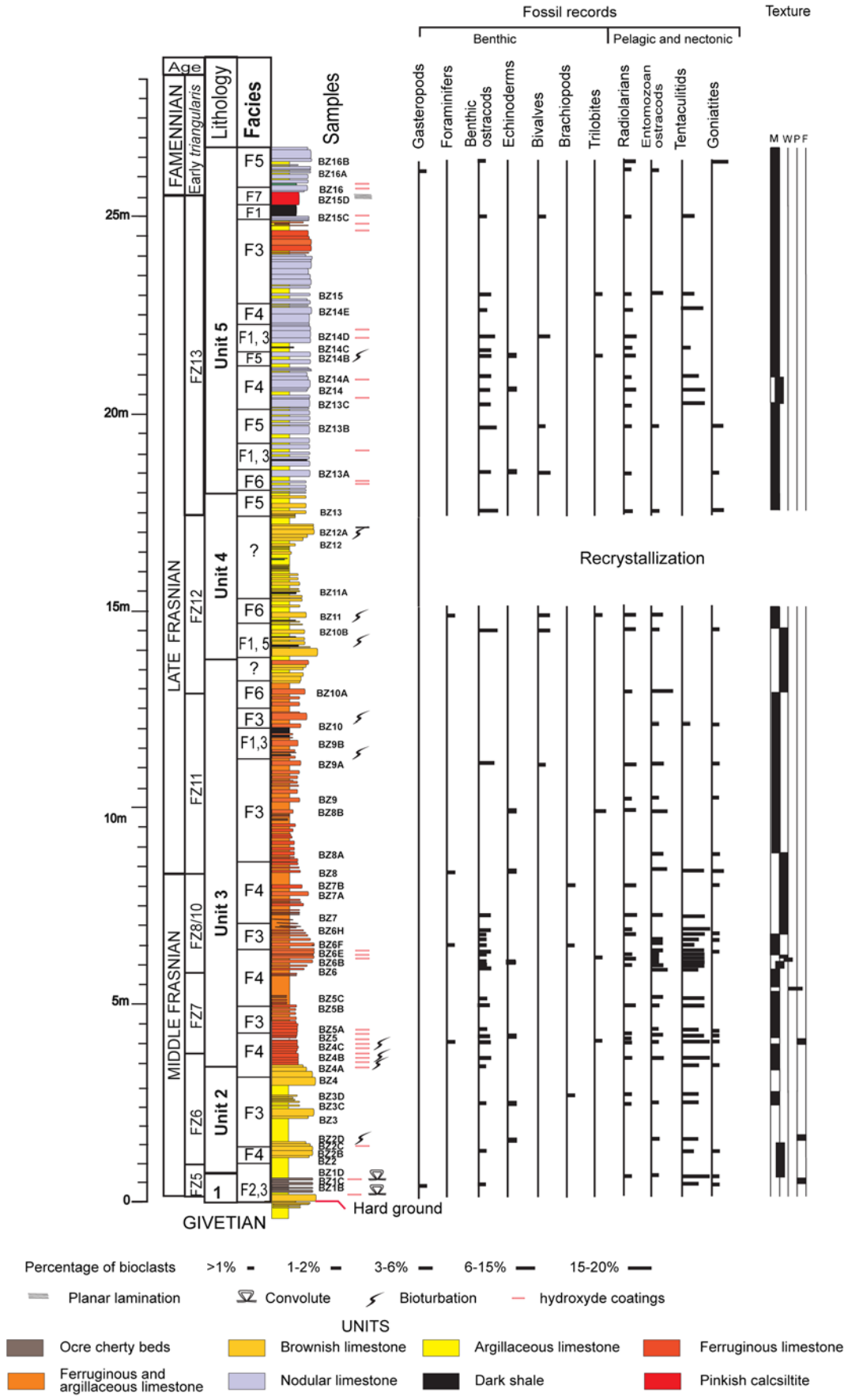

Fig. 2. (Colour online) Lithological column with relative abundance of fossil components and facies fabrics of the Ben Zireg section. Conodont zones from Mahboubi *et al.* (2015). Lithostratigraphic Unit 1: ochre cherty limestones with soft-deformations; Unit 2: massive micritic limestones; Unit 3: ferruginous limestones; Unit 4: pseudo nodular argillaceous limestones; Unit 5: nodular limestones. Abbreviations: M – mudstone; W – wackestone; P – packstone; F – floatstone; FZ – Frasnian conodont Zone (after Klapper & Kirchgasser, 2016). The recrystallization interval corresponds to carbonate deposits which suffered post-diagenetic processes and were recrystallized into microsparite to sparite; most of sedimentary features and fossils cannot be determined.

https://doi.org/10.1017/S0016756818000626 Published online by Cambridge University Press

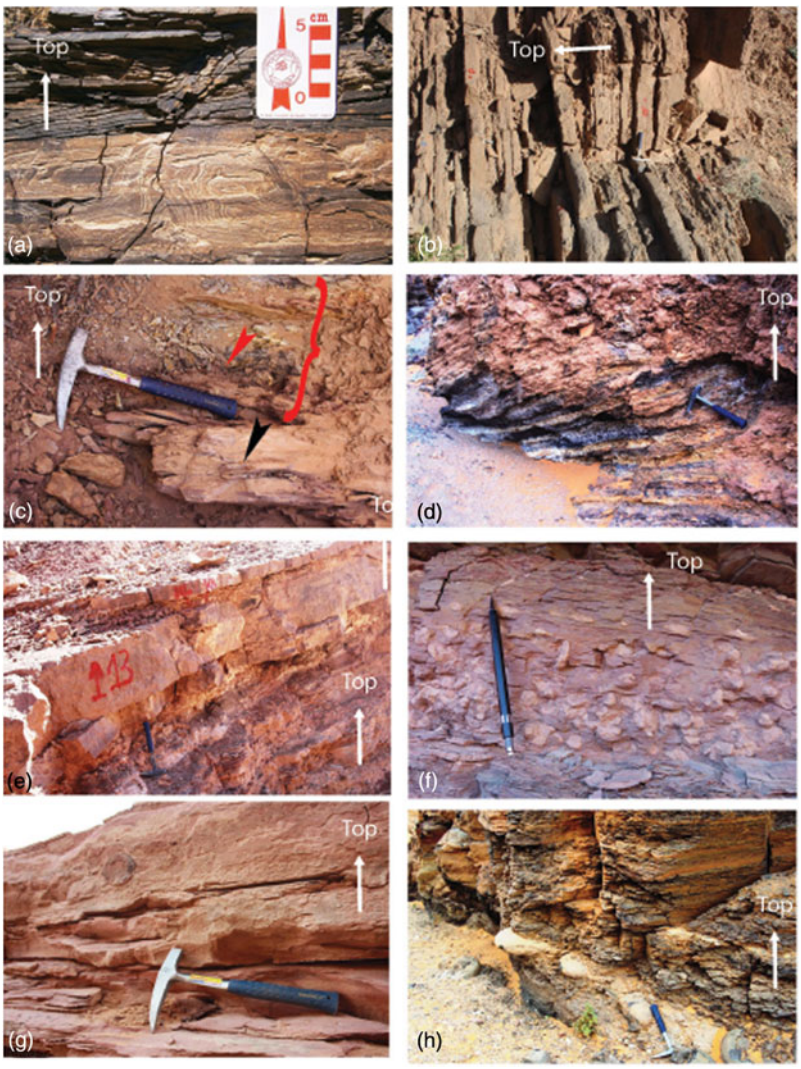

Fig. 3. (Colour online) Lithofacies. (**a**) Unit 1 at Ben Zireg, convolute laminations (Facies 2). (**b**) Unit 5 at Ben Zireg, thin-bedded, upper Frasnian micritic limestones (Facies 3). (**c**) Uppermost Unit 5 at Ben Zireg, detail of the upper Kellwasser bed with a layer of black shales (red arrow and bracket, Facies 1) superseded by laminated pinkish calcisiltic shale (black arrow, Facies 7). (**d**) Unit 1 at South Marhouma, blackish shales (Facies 1). (**e**) Unit 2 at South Marhouma, alternating Facies 6 pseudonodular limestone beds and Facies 1 grey shales. (**f**) Unit 3 at South Marhouma, cross-sectional view of interbedded Facies 3 argillaceous lime nodules. (**g**) Top of Unit 3 at South Marhouma, laminated black to pinky shales (Facies 7) of the upper Kellwasser bed. (**h**) Unit 4 at South Marhouma, decimetre-thick diagenetic limestones and Facies 1 dark shales from lower Famennian strata.

Unit 3 contains conodonts representative of the top of FZ8–10 to FZ13 (the latter with *Pa. bogartensis*) interval. It is characterized by unfossiliferous greenish and greyish shales with frequent reddish and greenish argillaceous nodular limestones (Fig. 3f) and some dark shale interbeds. The input of siliciclastic material increases towards the top, including millimetre-thick intercalations of parallel laminated sandstone. The upper Kellwasser horizon of this section is marked by plane-laminated shales (Fig. 3g).

Unit 4 contains conodonts representative of the early Famennian Age (*Pa. ultima*, *Pa. subperlobata*). It is mainly composed of decimetre-thick dark grey to black argillaceous nodular limestones, displaying large orthoceratids and brachiopods, and of unfossiliferous greyish laminated shales (Fig. 3h).

4.b. Facies

On the basis of differences in texture, fossil components and lithological nature, seven sedimentary facies (F1–7) are identified (Figs 2, 4). The original texture of most rocks was obscured or obliterated during burial and diagenesis, tectonic processes or both. Indeed, microshear zones and stylolites are locally identified within nodular limestones. Moreover, the original lime mud was minutely recrystallized (e.g. Fig. 5h, i).

4.b.1. Shale and calcareous nodules (F1)

In both sections, finely laminated greyish shales are interbedded with dark grey shales, calcareous shales or both. Bed thicknesses range from millimetres to a few metres. Thick layers of shales also display septaria nodules in the South Marhouma section, whereas such shales are less common at Ben Zireg. The faunal content is represented only by poorly preserved shelly pelagic organisms (e.g. tentaculites and bivalves).

4.b.2. Lithoclastic floatstone (F2)

This facies is uncommon and was found only at Ben Zireg. The lithoclasts mainly consist of chaotic, randomly organized angular to rounded limestone and cherty clasts (Fig. 5a, b). Carbonate clasts are composed of monomict, poorly sorted pelagic mudstones belonging to Facies 3 (see below). Lithoclasts are supported by a matrix composed of lime mud, clay, microsparite and iron hydroxide. Recrystallized millimetre-thick siliceous laminae can locally occur. The fossil components consist of rare pelagic ostracods (entomozoans) and tentaculite debris. Inverse grading in the lower part of some decimetre-thick beds was observed.

4.b.3. Poorly fossiliferous mudstone (F3)

This facies is common in both sections. In the South Marhouma section, F3 is found in Units 1 and 3 consisting of greyish nodular,

https://doi.org/10.1017/S0016756818000626 Published online by Cambridge University Press

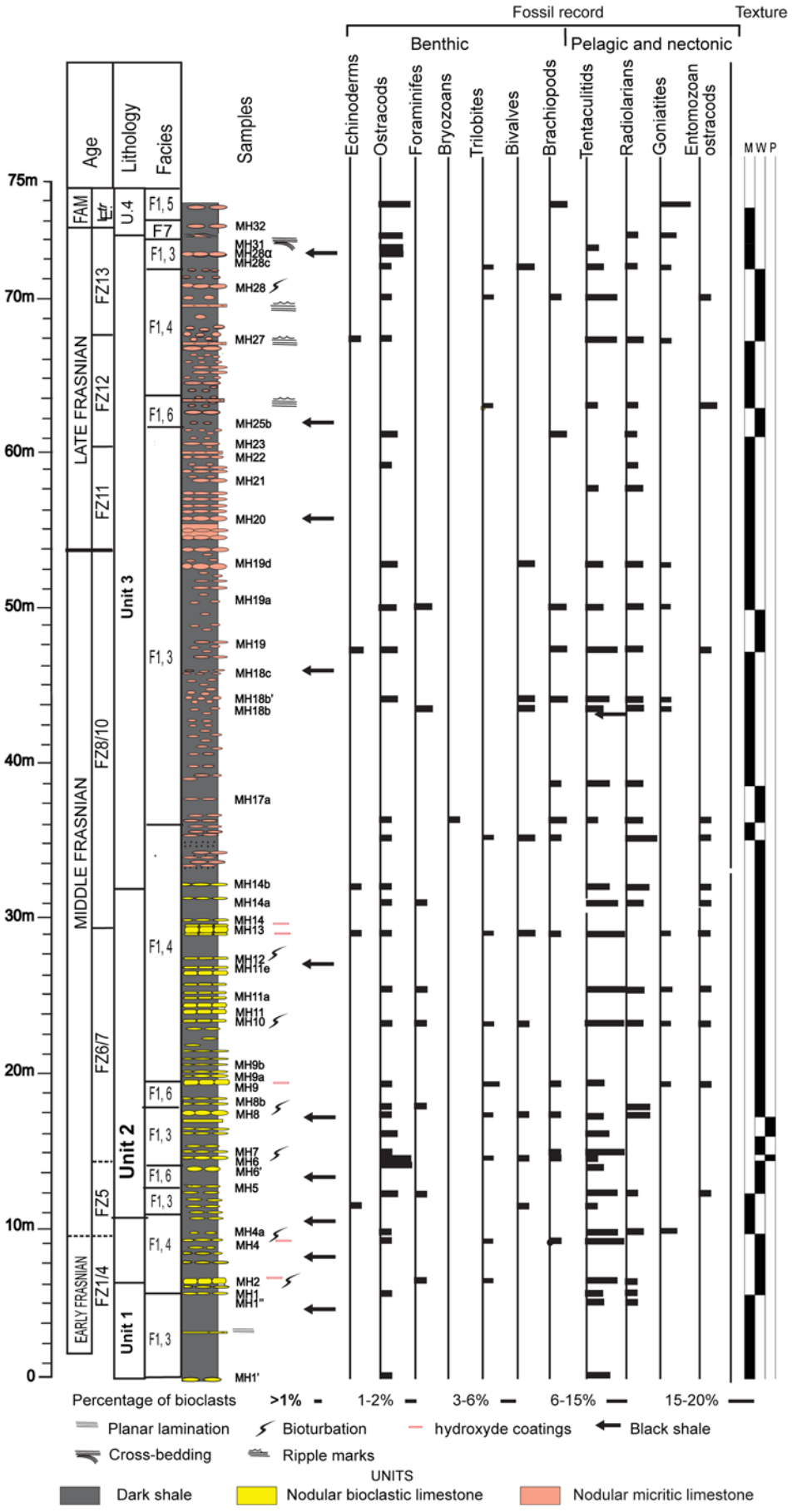

Fig. 4. (Colour online) Lithological column with relative abundance of fossil components and facies fabrics of the South Marhouma section. Conodont zones from Mahboubi & Gatovsky (2014). Lithostratigraphic Unit 1: dark shales; Unit 2: bioclastic nodular/pseudonodular limestones, grey shales; Unit 3: nodular muddy limestones, greenish/darkish shales; Unit 4: diagenetic limestones, black shales. Abbreviations: L.*tr*. – lower *triangularis*; FAM – Famennian; and as for Figure 2.

https://doi.org/10.1017/S0016756818000626 Published online by Cambridge University Press

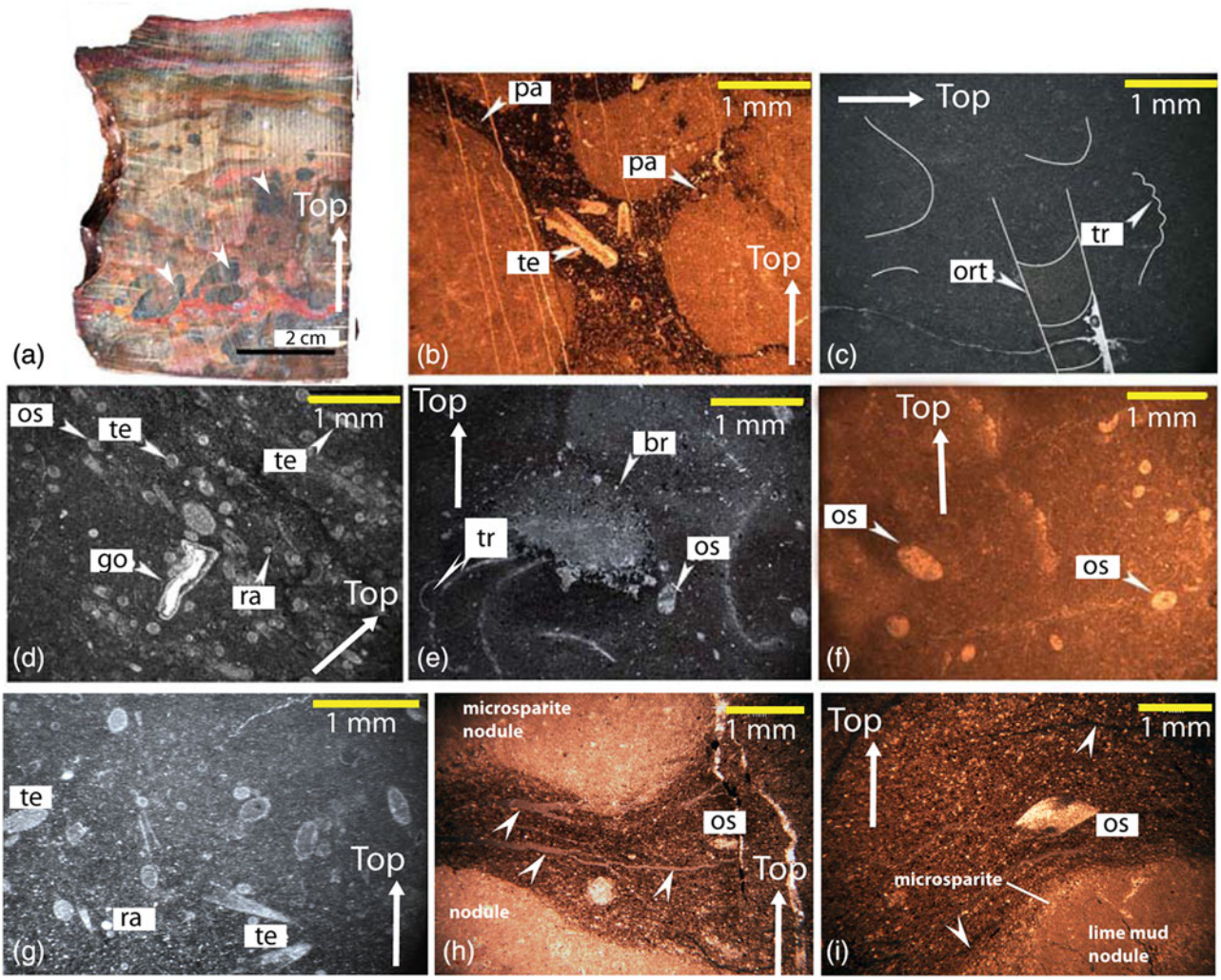

Fig. 5. (Colour online) Facies of the depositional environments of the South Marhouma section and the Ben Zireg section: (a) hand sample and (b–i) thin-sections. (**a**) Facies 2, outer-ramp deposit: reworked mudstone layers in the Ben Zireg section (bed BZ2B). (**b**) Facies 2, outer-ramp deposit: zoom on reworked mudstone layers (bed BZ1C). (**c**) Facies 6, mid–outer-ramp deposit: lime mudstone with cephalopod bioclasts (bed MH34). (**d**) Facies 4, outer-ramp deposit: pelagic argillaceous wackestone displaying distinct lamination by parallel arrangement of tentaculite coquinas (bed MH10). (**e**) Facies 6, mid–outer-ramp deposit: diversified wackestone with bioclasts consisting of abundant brachiopod shells (bed MH32). (**f**) Facies 6, mid-ramp deposit: fine-grained mudstone with benthic ostracods (bed BZ10B). (**g**) Nodule of carbonate Facies 3 within shales of Facies 1, outer-ramp deposit: fine-grained wackestone with randomly orientated tentaculites and radiolarians (Bed MH 28). (**h**) Recrystallized nodule of Facies 3 in Facies 1: lime mud transformed into microsparite; note tension gashes filled by calcite (arrow). (**i**) Nodule of Facies 3 in Facies 1: lime mud partially transformed into microsparite in the margin; note pressure-solution surfaces underlined by oxide concentrations (arrow). Abbreviations: br – brachiopod; go – goniatite; ort – orthoceras; os – ostracod; pa – parabreccia; ra – radiolarian; tr – trilobite; te – tentaculite.

centimetre-thick lime beds in shale. Nodules consist of lime mud and wackestone partially or totally transformed into microsparite (Fig. 5h, i). In the Ben Zireg section it occurs mainly in Units 3 and 5 as centimetre-thick fine-grained limestone beds or greyish nodular limestones, respectively. The matrix of this facies is lime mud or microsparite. Micritic limestones lack bioturbation fabrics, whereas burrowing traces are sometimes observed in nodular limestones embedded within greyish shales. F3 is characterized by poor faunal content that is locally represented by pelagic organisms such as tentaculites, pelagic bivalves, entomozoans and radiolarians (Fig. 5g). No current fabrics have been macroscopically observed in this facies.

4.b.4. Argillaceous wackestone (F4)

This facies occurs mainly in middle Frasnian strata in both sections. It comprises centimetre- to decimetre-thick greyish to reddish limestones. Pressure-solution processes commonly triggered tectonic stylolithization. The common type of texture is wackestone with microbioclasts occurring in a patchy distribution. The matrix therefore displays ferruginous blisters organized into isolated or grouped, concentric internal structures. Submicrometric hydroxide grains are often found. Beds are frequently coated at the top with films of iron hydroxides. The faunal content is commonly abundant, with tentaculites as the dominating organisms followed by entomozoans, radiolarians, cephalopods and pelagic bivalves (Fig. 5d). Additionally, scarce benthic faunas are represented by debris of trilobites, brachiopods and ostracods. Bioclasts are generally poorly sorted; they can be concentrated into millimetre-thick laminations with a random distribution of fossils, and are partially affected by bioturbation.

4.b.5. Diversified fauna mudstone to wackestone (F5)

This facies is most commonly found in the uppermost part of both sections. In the South Marhouma section, it is composed of large

https://doi.org/10.1017/S0016756818000626 Published online by Cambridge University Press

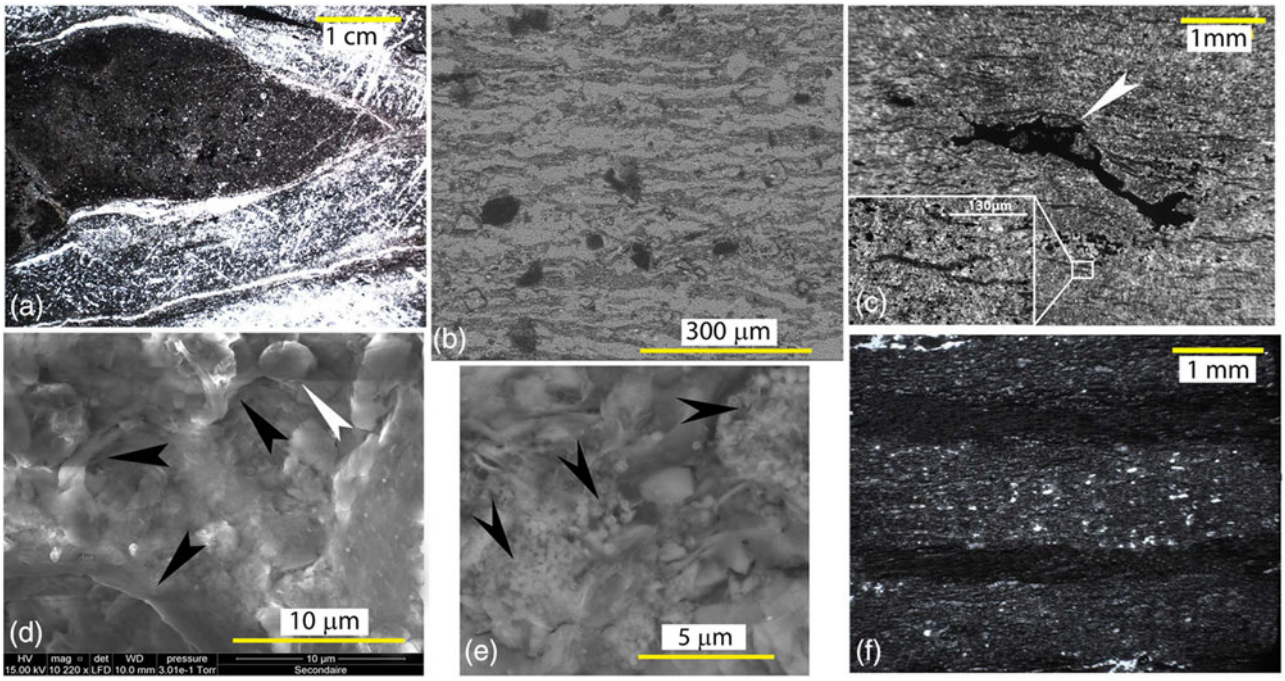

Fig. 6. (Colour online) Facies 7, mid-ramp deposits, uppermost Frasnian strata at South Marhouma and Ben Zireg sections. (**a**) Flat pebble conglomerate fabric (bed MH26bas). (**b, c**) SEM image of kerogenous laminae (wavy-crinkly structures) (bed MH29). (**d**) SEM image of tube-like structures (black arrows) and possible coccoid structure (white arrow) (arrows, bed BZ15D). (**e**) Framboidal pyrite (arrows, bed MH29). (**f**) Finely laminated striped shale displaying silt–mud couplets (bed MH30).

dark microsparitic nodules of early *triangularis* Zone age. In the Ben Zireg section, the same facies consists of greyish nodular muddy limestones. Fossil components are dominated by nektonic faunas such as cephalopods including *Orthoceras*, mostly fragmented and poorly preserved (Fig. 5c). Pelagic organisms, radiolarians, entomozoans and tentaculites are less frequent. Benthic faunas are more abundant compared with Facies 4 (Fig. 5e); they are dominated by ostracods and the skeletal debris of echinoderms, brachiopods and trilobites. This facies is locally bioturbated. Geopetal structures are recognized within ostracods and cephalopods coquinas.

4.b.6. Lime ostracod mudstone (F6)

This facies is not frequent in the studied sections (samples BZ10a, BZ11, BZ13a and MH6′). It occurs mostly in FZ12 in the Ben Zireg section. It consists of yellowish thin-bedded argillaceous limestones. The matrix is microsparite to sparite, rarely containing euhedral replacement of dolomite crystals. The bioclastic components of this mudstone consist predominantly of benthic ostracods (Fig. 5f), followed by trilobite and brachiopod fragments. Additionally, pelagic elements are limited to entomozoans, radiolarians and recrystallized fragments attributed to pelagic molluscs. Lime mud geopetal infillings are sometimes observed. The systematic study of benthic ostracods from acid residues revealed the presence of the suborders Podocopida and Metacopida, related to Assemblage III of Casier (2008).

4.b.7. Microbial (?) shale (F7)

This facies is found only in the uppermost part of the studied sections, below the Frasnian–Famennian boundary (Figs 2, 4). It is exhibited in the South Marhouma section as lenticular centimetre- to decimetre-thick dark, carbonaceous to silty shale. The texture is close to the striped shale facies of Schieber (1989), with silt and mud couplets (light) alternating with carbonaceous silty shale (dark) (Fig. 6f). In petrographic thin-section, the texture displays discontinuous wavy-crinkly laminae of kerogenous matter that are associated with framboidal pyrites and cubic euhedral crystals (Fig. 6b, c, e). Terrigenous quartz grains, isolated mud fragments and imbricated flat pebbles can also be found (Fig. 6a). Characteristic organisms are reworked benthic ostracods, rare brachiopods and undetermined mollusc shells.

In the Ben Zireg section, the microbial (?) shale facies is observed in bed BZ15D (uppermost FZ13). It consists of pink, laminated, calcareous, silty shale. The thin-sections display a fine-grained matrix with abundant dolomite crystals and rare mica crystals. The wavy-crinkly laminae described above are discrete and are organized into submicrometric- thick kerogenous units alternating with fine-grained calcareous laminae. SEM observations display tube-like shapes locally forming ramiform structures, possible coccoid structures (Fig. 6d) and some framboidal pyrite. Fossils are very sparse, with brachiopods, benthic ostracods and tentaculite fragments.

4.c. MS trends

Our measurements of MS (Figs 7, 8) provided extremely low values for the Frasnian and basal Famennian strata. These vary between 0.1 and 8×10^{-8} m^3 kg^{-1} at the South Marhouma section with an empirical average value of 1.9×10^{-8} m^3 kg^{-1}. They are even lower in the Ben Zireg anticline, where they fluctuate between 0.4 and 3.7×10^{-8} m^3 kg^{-1} with an average of 1.3×10^{-8} m^3 kg^{-1}. Although MS values are low, they are consistent with results from other localities of similar ages. In both Algerian sections, the averages of MS values are lower than those for the MS_{marinestandard} (5.5×10^{-8} m^3 kg^{-1}) of Ellwood *et al.* (2011) and Da Silva *et al.* (2009). This was also observed in the

https://doi.org/10.1017/S0016756818000626 Published online by Cambridge University Press

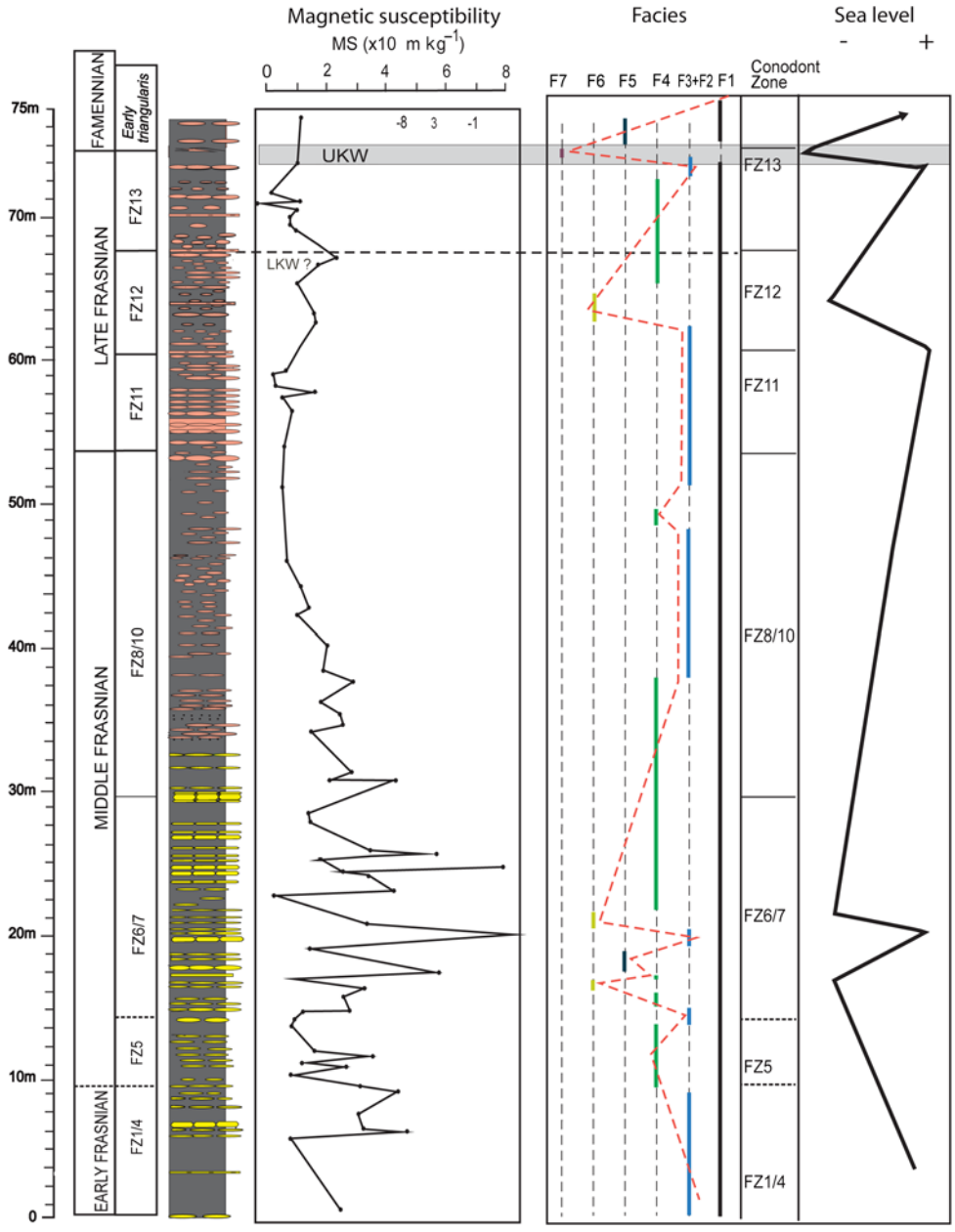

Fig. 7. (Colour online) Magnetic susceptibility evolution, facies change and sea-level fluctuations through the Frasnian strata in the South Marhouma section. Abbreviations: LKW – lower Kellwasser; UKW – upper Kellwasser; and as for Figure 2. Stippled line: assumed position of the LKW.

Carnic Alps (Pas *et al.* 2014) and in the Dinant Synclinorium (Pas *et al.* 2015), where mean values range over 0.1–1 × 10^{-8} m^3 kg^{-1}. In contrast, values are highly variable in the Frasnian deposits of western Canada (Whalen & Day, 2010). Low values are mainly recorded during late transgression and early highstand intervals, and MS signature is generally lower in platform settings than in basinal settings.

Qualitative analysis of the MS data suggests the same global trend with shared peaks, which are considered as isochronous (Crick *et al.* 2001) in the South Marhouma and Ben Zireg sections (Figs 7, 8). At South Marhouma, the lower part of the section from FZ1–4 to FZ6–7 shows fluctuations in MS value from 0 to 8 × 10^{-8} m^3 kg^{-1}. The upper part of the section, from FZ8–10 to the Famennian strata, shows low values between 0 and 3 × 10^{-8} m^3 kg^{-1}. At Ben Zireg, the lower part of the section from FZ5 to FZ7 shows little fluctuation between 0 and 3 × 10^{-8} m^3 kg^{-1}. In the upper part of the section, from FZ8–10 to the Famennian strata, the MS value remains low between 0 and 1 × 10^{-8} m^3 kg^{-1}.

5. Discussion

5.a. Facies interpretation

5.a.1. Shale and calcareous nodules (F1)

Shales such as those at the base of the South Marhouma section (Fig. 3d) are usually interpreted as representing deposition in deep basin settings (e.g. Boulvain *et al.* 2004), but recent sedimentological investigations indicate that mudrocks may also have been deposited under current activity from proximal to distal parts of shelves (e.g. Schieber *et al.* 2007; Bohacs *et al.* 2014). At South Marhouma, calcareous nodules within shales are lime mudstone to wackestone and frequently display randomly orientated pelagic bioclasts, tentaculites and microspheres interpreted as calcitized radiolarians (Fig. 6g). F1 is therefore interpreted as the deepest

https://doi.org/10.1017/S0016756818000626 Published online by Cambridge University Press

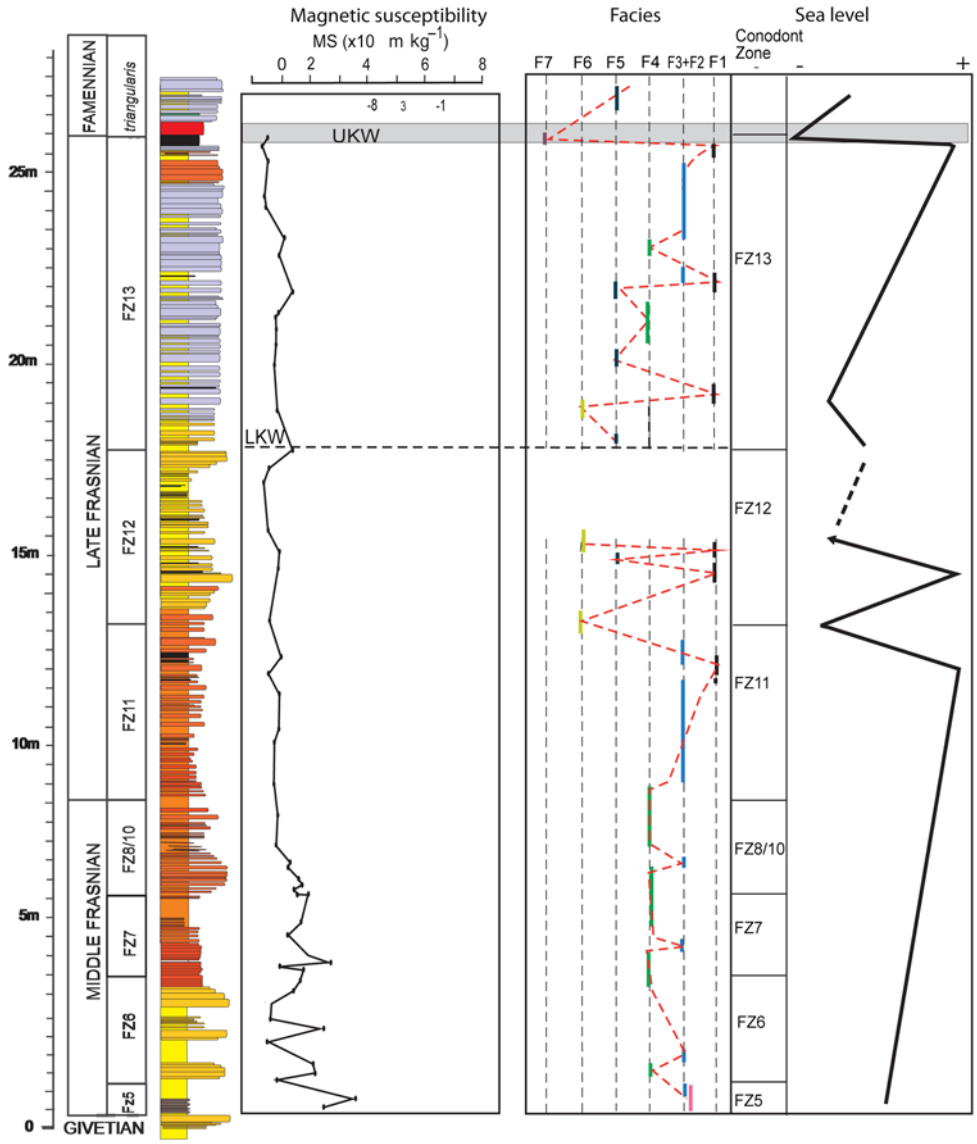

Fig. 8. (Colour online) Magnetic susceptibility evolution, facies change and sea-level fluctuations through the Frasnian strata in the Ben Zireg section. Abbreviations as for Figure 7. Stippled line: assumed position of the LKW.

facies in the Frasnian interval, deposited below storm wave-base. This facies is common in the Frasnian deposits in North Africa (e.g. Ahnet and Mouydir basins; Lüning *et al.* 2004; Wendt *et al.* 2006), sometimes associated with organic matter (Boote *et al.* 1998). Grey shale can locally change into black shale intervals, the latter interpreted as deposited in dominantly dysoxic setting with variable amounts of free hydrogen sulphide in the sediments (e.g. Boyer *et al.* 2011). Brief episodes of anoxia may occur in this depositional setting. Such conditions may be found in different places on epeiric platforms, even in shallow-water deposits (Boyer & Droser, 2009; Boyer *et al.* 2011), but at South Marhouma they are interpreted as having been emplaced in a deep-sea setting within F1.

5.a.2. Lithoclastic floatstone (F2)

This facies was assigned to seismo-turbidites by Mutti *et al.* (1984) or megaturbidites by Cook *et al.* (1972). In our case, this facies is restricted to Unit 1 of the Ben Zireg section in association with convolute bedding, and corresponds to debris flows into a distal pelagic domain. This facies may also correspond to gravitational deposits that formed under low sedimentation rates and tectonic activity (Rossetti & Góes, 2000). Convolute structures associated with reworked lithoclasts can be generated by seismic shocks giving rise to downslope movements (Spalletta & Vai, 1984). F2 is similar to facies described elsewhere in the Upper Devonian successions from the Eastern Anti-Atlas (Wendt & Belka, 1991).

5.a.3. Poorly fossiliferous mudstone (F3)

The fine-grained matrix with rare fossils suggest low-energy and open-marine conditions, remaining below storm wave-base (Pas *et al.* 2013, 2014). The scarcity of bioturbation could reflect oxygen-depleted waters (Flügel, 2004). Nodules are composed of lime mudstone to wackestone (Fig. 5h, i) which suffered partial to complete transformation into microsparite. They are considered as late diagenetic in origin (James & Choquette, 1990).

5.a.4. Argillaceous wackestone (F4)

On the basis of the abundance of pelagic fossils, facies F4 is interpreted as having been deposited in a deep-water environment, below storm wave-base (Pas *et al.* 2013, 2014). Finely laminated biogenic detritus is interpreted as having been deposited by turbidity currents or distal tempestites (*sensu* Aigner, 1985).

https://doi.org/10.1017/S0016756818000626 Published online by Cambridge University Press

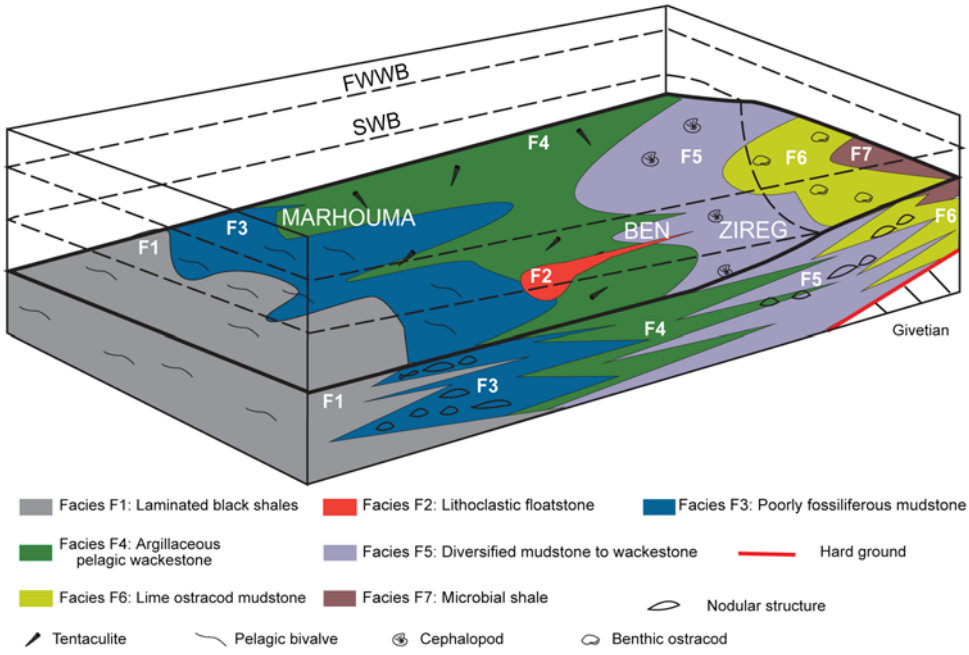

Fig. 9. (Colour online) Sedimentary model in NW Algeria through the Frasnian Stage (South Marhouma and Ben Zireg sections). This model shows a mid- to outer-ramp setting with lateral distribution of facies from the most proximal setting (F7) to the most distal (F1). Abbreviations: SWB – storm wave-base; FWWB – fair-weather wave-base.

Iron hydroxide grains within the matrix may result from anaerobic bacteria activity in the uppermost part of the sediment (Mamet & Préat, 2006).

5.a.5. Diversified fauna mudstone to wackestone (F5)

Compared with F4, the increase in both benthic faunal diversity and bioturbation, typical of areas with normal oxygen concentration (Flügel, 2004), in F5 indicates that the depositional setting of this facies was predominantly below storm wave-base action, but shallower than for F4.

5.a.6. Lime ostracod mudstone (F6)

The frequent occurrence of disarticulated ostracods may suggest para-autochthonous aggregations produced by episodic storm-induced seafloor disturbances (Schülke & Popp, 2005). The increase in benthic fauna and the ostracod assemblage might also indicate a more proximal depositional setting compared with the previous environment, likely between the fair-weather wave-base and the storm wave-base.

5.a.7. Microbial (?) shale (F7)

Framboidal pyrite is commonly present in hypoxic to anoxic environments (e.g. Bond *et al.* 2004; Peckmann & Thiel, 2004; Wignall *et al.* 2005; Tian *et al.* 2014) where crystallization is partly controlled by bacterial activity (e.g. Folk, 2005; MacLean *et al.* 2008). The association of wavy-crinkly structures with kerogen laminae has been considered as resulting from the occurrence of benthic microbial (cyanobacterial?) mats (e.g. Schieber, 1986, 1989; Sur *et al.* 2006; Deb *et al.* 2007) and coccoidal bacteria that have been identified within such deposits (Kaźmierczak *et al.* 2012). Even if no obvious diagnostic feature of primary cyanobacterial mats (e.g. web-like texture indicator of benthic coccoidal remnants, Kremer & Kaźmierczak, 2005) were found in the studied sections, the presence of organic matter, framboidal pyrite, wavy lamination, wavy lenticular lamination with shale fragments, wavy-crinkly structure, possible coccoid structure and submicrometric tubular structures are strongly suggestive of the presence of microbial mats during the deposition of the dark shales in the two sections. The presence of mud and silt couplets with locally reworked fossils indicates fluctuating high-energy episodes attributed to storms. Such an interpretation is compatible with that of Schieber (1986, 1989) who located the depositional environment of similar shales between fair-weather wave-base and average storm wave-base.

5.b. Local depositional environment

Palaeoenvironmental interpretations of the depositional settings of F1 and F3–7 observed in both sections (plus F2 at Ben Zireg only) support the interpretation that the sediments were deposited along a low-angle, mid- to outer-ramp profile *sensu* Wright & Burchette (1996) on a regional scale (Fig. 9).

5.b.1. Ben Zireg section

The section is dominated by fine-grained carbonates above a major gap in the lower Frasnian strata. From FZ5 to FZ11 sedimentation resumed in autochthonous Facies 1 and 3 and allochthonous Facies 2, which are the deepest facies (Fig. 2). Primary iron hydroxide coatings at the top of the lime beds are common. The lower Frasnian gap corresponds to a non-deposition and possibly erosion in a submarine setting, and has been related elsewhere to bottom currents (Hüneke, 2006). There is no evidence of the presence of such currents at Ben Zireg. Indeed, features such as erosional surfaces, coarsening-upwards and fining-upwards micro-sequences, and limestone with orientated tentaculitid, laminated calcisiltites, phosphatic grains, phosphorites and phosphatic hard-grounds (Hüneke, 2013) have not been found. From FZ11 to lower FZ13, shallower Facies 5 and 6 alternate with the deep Facies 1. From lower to upper FZ13, Facies 5 and 6 are replaced by deeper Facies 4 and 3. The shallowest Facies 7 was deposited within the uppermost FZ13, (upper Kellwasser), below the Frasnian–Famennian boundary.

An outer-ramp model is suggested for this area at the northern margin of the Algerian Sahara (Fig. 9). In this model, the deepest deposits are represented by some grey to black shale intervals (Facies 1, Fig. 3d) and siliceous deposits with convolute lamination

https://doi.org/10.1017/S0016756818000626 Published online by Cambridge University Press

and breccias (Facies 2; Figs 3a, 5a, b). In our model (Fig. 9), Facies 4 and 5 were emplaced below storm wave-base, as no current features were found. Common ferruginous coatings point to repeated episodes of hydroxide cementation on the sea floor. The proximal part of the ramp displays accumulations of fragmented bioclasts from both benthic and pelagic communities. This is interpreted as indicating deposition between storm wave-base and fair-weather wave-base, with an increasing amount of benthic fauna from Facies 5 to shallower Facies 6. The overall stratigraphic trend estimated at Ben Zireg from broad lithologic trends indicates a deep-sea depositional setting disrupted by a shallower setting within FZ12, the lower part of FZ13 and at the top of FZ13.

5.b.2. South Marhouma section

This section is dominated by mudrocks (e.g. shales) and fine-grained carbonate deposits with mostly pelagic, open-marine fauna.

From FZ1 to FZ4, sedimentation resumed in autochthonous Facies 1 and 3 which are the deepest facies (Fig. 4). Facies 2 was not found. From FZ5 to FZ13, the nodular argillaceous limestones (Facies 3) with mudstone texture and rare fauna suggest distal depositional setting under quiet conditions. The fine-grained bioclastic mudstone and wackestone (Facies 4) with an overwhelming abundance of pelagic marine fauna still supports a quiet depositional setting but in shallower waters. A shallower ramp is recognized within FZ6–7 and FZ12 by the increase of benthic faunal components (Facies 5 and 6). The shallowest facies is represented here by the occurrence of microbial (?) benthic mats (Facies 7) that are affected by storm action below the fair-weather wave-base. In summary, the broad lithologic trends indicate a deep-sea depositional setting, with shallower intervals during the deposition of FZ5–7, FZ12 and uppermost FZ13.

5.b.3. Comparison between sections

Stratigraphic correlation between Ben Zireg and South Marhouma is documented in Mahboubi *et al.* (2015). The Frasnian deposits of the South Marhouma section are nearly three times thicker than those of Ben Zireg, although mostly represented by shale deposits of Facies 1. The highly expanded section at South Marhouma is interpreted as indicating a higher sedimentation rate in the subsiding basin closer to the source (the West African Craton, Fig. 1a). In contrast, condensed carbonate deposits with minor shaly interbeds and frequent hydroxide coatings characterize Ben Zireg, where shallower Facies 3–5 dominates. Such a depositional setting results either from submarine positive relief (shoal) or from a more distal location to the source areas of detrital inputs.

5.c. Sea-level fluctuations

Integrating both lithofacies and MS data (Figs 8, 9), as well as data of conodont biofacies (Seddon & Sweet, 1971; Sandberg, 1976; Klapper & Barrick, 1978; Sandberg & Ziegler, 1979) published on both studied sections (Mahboubi & Gatovsky, 2014; Mahboubi *et al.* 2015), we tentatively interpret environmental changes through middle–late Frasnian time in terms of bathymetrical variation.

Our MS data were collected in the same kind of depositional setting (outer to mid ramp) and, during diagenesis, we did not observe dolomitization or hydrocarbon migrations, suggesting that the MS results are related to primary signal. Nevertheless, MS data do not seem to clearly record variations in sea level consistent with the other proxies, especially within FZ8–13 where MS values remain very low (Figs 7, 8).

5.c.1. Early Frasnian

During early Frasnian time (FZ1–4), the South Marhouma section displays a regressive trend with an upwards change from Facies 1 to 3 and fluctuating MS values that are consistent with regression (Fig. 7). This trend is in contradiction to the transgressive trend recorded in North America at that time (Fig. 10). It could be related to the specific location of the South Marhouma section, where abundant fine-grained siliciclastic inputs from the emerging West African Shield might have obscured the eustatic signal.

5.c.2. Middle Frasnian

Between FZ5 and the beginning of FZ8–10, both sections display fluctuations in the MS signal and lithofacies (Figs 7, 8). Within this interval, slight shifts in MS values at South Marhouma roughly reflect concomitant shifts in lithofacies. In contrast, shifts in both MS and lithofacies, although discernible, are less pronounced at Ben Zireg. In particular, MS values, which vary between 0 and 8×10^{-8} m^3 kg^{-1} at South Marhouma, are much lower at Ben Zireg with a shift from 1 to 3×10^{-8} m^3 kg^{-1}, being almost insignificant. In parallel, variations in succeeding lithofacies are more frequent with shifts from Facies 1 to 6 at South Marhouma, whereas these are restricted to Facies 2 and 3 and Facies 4 at Ben Zireg. The mean prevalence of Facies 4 in both sections, along with a weak decrease in MS values, coincides with biofacies indicators available at Ben Zireg that shift temporarily from shallower *Polygnathus–Icriodus* biofacies in FZ6 to deeper *Polygnathus* biofacies between FZ7 and the beginning of FZ8–10, before returning to *Polygnathus–Icriodus* biofacies thereafter (Mahboubi *et al.* 2015).

During middle Frasnian time the global trend is transgressive (Johnson & Sandberg, 1988; Sandberg *et al.* 1992; Filer, 2002; Morrow & Sandberg, 2008), with important deepening during the deposition of FZ5–6 (*punctata* Event) (Pisarzowska & Racki, 2012). In the nearby Tafilalt region, the global transgressive trend is documented from FZ8 (Dopieralska *et al.* 2016) and culminates at the end of FZ10 (Fig. 10). This global trend is likewise observed at Ben Zireg. At South Marhouma, the global transgressive trend begins in the lower part of FZ6–10 but a marked regressive event occurred at the transition between FZ6 and FZ7.

5.c.3. Late Frasnian

MS values remain constantly very low within upper Frasnian strata without any significant changes at the upper Kellwasser level in particular, and such values cannot be related to transgression only. The reasons for such stable low values remain unknown.

Within the lower FZ11, facies changes indicate a regressive event followed by a transgressive peak in the upper FZ11. This transgressive peak is characterized by a significant extension of deep-sea lithofacies, associated with conodont records dominated by biofacies *Polygnathus–Palmatolepis*. This signal is most obvious at Ben Zireg (Mahboubi *et al.* 2015), whereas at South Marhouma the paucity of available conodont records prevents confirmation of the slight deepening of the sedimentary setting (Mahboubi & Gatovsky, 2014). The curve of Ben Zireg remarkably coincides with the curves obtained in Euramerica and in the Tafilalt (Fig. 10). At South Marhouma, only the transgressive peak is clearly recorded. Dopieralska *et al.* (2016) emphasize the importance of the *semichatovae* transgression with the highest positive shift in ε_{Nd} values within FZ11. This event has earlier been described in Euramerica, where it is characterized by the sudden spread of *Palmatolepis semichatovae* in FZ11 (Sandberg *et al.* 1992, 2002). This species has not been established in the studied sections, but

https://doi.org/10.1017/S0016756818000626 Published online by Cambridge University Press

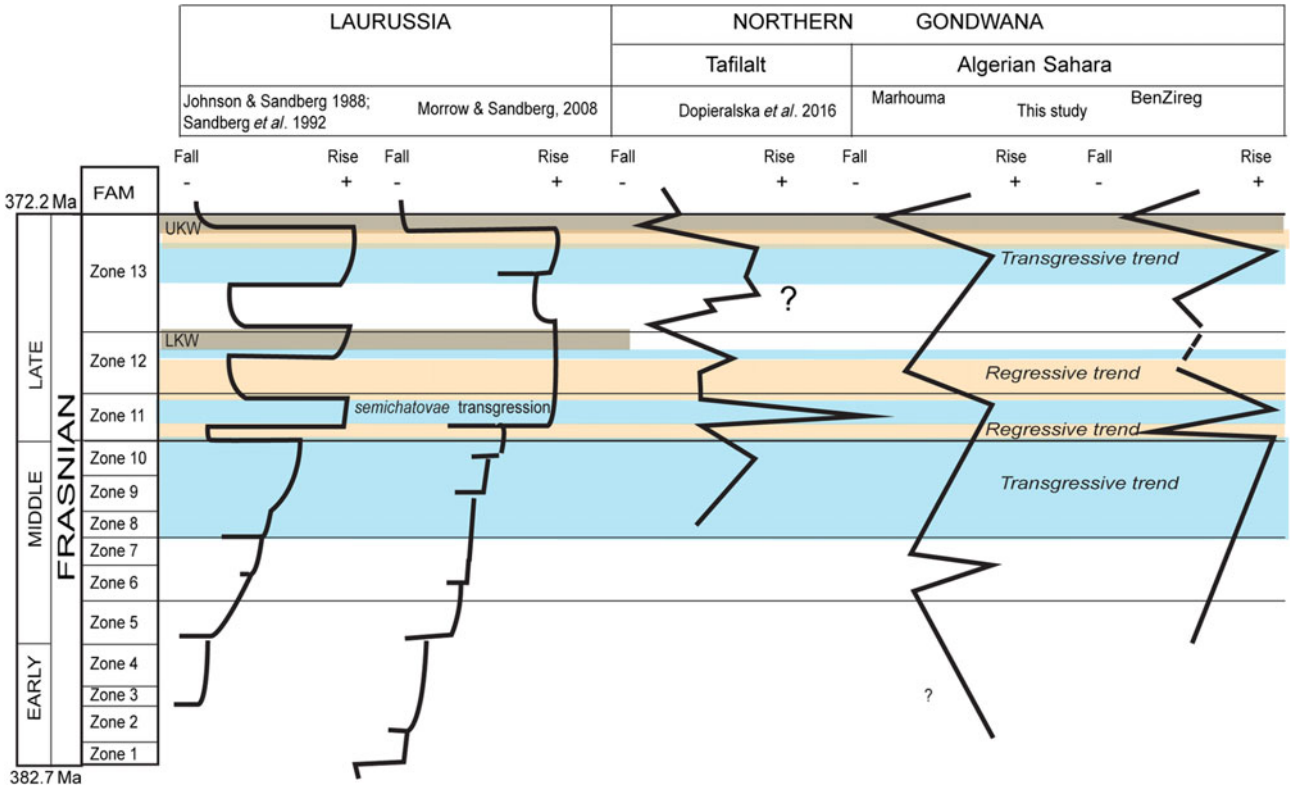

Fig. 10. (Colour online) Comparison of sea-level fluctuations from Laurussia and northern Gondwana through the Frasnian Stage. FZ (Frasnian Zones) after Klapper & Kirchgasser (2016), relative duration of conodont Zones are from Becker *et al.* (2012). In grey: anoxic events. UKW: Upper Kellwasser; LKW: Lower Kellwasser; FAM: Famennian.

the obvious transgressive episode recorded within FZ11 at both South Marhouma and Ben Zireg may most likely correspond to this event. As a whole, evidence of the *semichatovae* transgression (Sandberg *et al.* 1992) is observed in the Saharian Platform.

During deposition of FZ12, evidence of shallower environments is provided by the deposition of Facies 5 and 6 at Ben Zireg and Facies 4–6 interbeds within Facies 1 at South Marhouma. Biofacies in both sections clearly indicate a shallowing trend with predominance of *Polygnathus–Ancyrodella* (Mahboubi & Gatovsky, 2014; Mahboubi *et al.* 2015). This regressive trend was also identified in Euramerica and in the Tafilalt (Fig. 10).

At the top of FZ12 and the transition between FZ12 and 13, the hypoxic lower Kellwasser horizon, usually occurring elsewhere, is not developed in its typical shale facies in our sections. Litho- and biofacies indicate an increase in water depth followed by fluctuations of lithofacies with an increase in water depth up to the upper Kellwasser horizon. Indicators of concomitant biofacies appear to be somewhat contradictory regarding this increase in water depth: they remain constant in terms of prevalence of *Palmatolepis–Polygnathus* and *Palmatolepis* at Ben Zireg, but return to shallower signals at South Marhouma with *Polygnathus–Ancyrodella* (Mahboubi & Gatovsky, 2014; Mahboubi *et al.* 2015). The increase in bathymetry observed in our sections is in accordance with that of Euramerica and Tafilalt (Fig. 10). Dopieralska *et al.* (2016) also identified regressive trends coinciding in particular with the early and late Kellwasser extinction events at the FZ12–13 transition and at the top of FZ13, respectively. In the studied sections, the regressive trend occurs slightly earlier within FZ12 when biofacies *Polygnathus–Ancyrodella* dominate. The lower Kellwasser deposits have been related to large-scale enhanced productivity and stratification of sea waters (Riquier *et al.* 2005). The anomaly we observed in Algeria might perhaps be the result of regional controls that could have complicated the biological/sedimentological signal. Furthermore, this part of the successions lacks precise stratigraphic controls; a precise location of the lower Kellwasser equivalent deposit is not yet possible. Thereafter, 'normal' transgressive conditions match the global sea-level trend. The upper Kellwasser horizon is characterized by its typical hypoxic facies at Ben Zireg. Bathymetric criteria point to a relative highstand of sea level at the beginning of the event, followed by a marked decrease of water depth until its top with the development of *Palmatolepis–Ancyrodella* biofacies (Mahboubi *et al.* 2015) and occurrence of possible 'microbial shales' (F7). In contrast, at South Marhouma, the drop in sea level seems to start earlier when Facies 7 and *Polygnatus–Icriodus* conodonts are present at the beginning of the presumed upper Kellwasser horizon (Mahboubi & Gatovsky, 2014). Consequently, it cannot be excluded that the equivalent of the late Kellwasser event started a little earlier at South Marhouma than considered by Mahboubi & Gatovsky (2014). At top of FZ13, the major regression during the upper Kellwasser horizon occurs both at Ben Zireg and South Marhouma, and is in accordance with the results of Johnson & Sandberg (1988) and Dopieralska *et al.* (2016).

5.c.4. Summary

The bathymetric curves on the Saharian Platform display a continuing sea-level rise through middle Frasnian time. A minor regression occurred within FZ6 at South Marhouma (Facies 3 shifts to Facies 6, consistent with the highest MS values), in accordance with the results of Pisarzowska & Racki (2012). A regression also

https://doi.org/10.1017/S0016756818000626 Published online by Cambridge University Press

occurred at the base of FZ11: at Ben Zireg, Facies 1 changes upwards into Facies 6, but MS values remain constantly low. During late Frasnian time in Euramerica, the global transgressive event achieved its highest stand from FZ11 to FZ13 (e.g. Morrow & Sandberg, 2008). This is matched by the recently established curve based on Nd isotopic data presented by Dopieralska *et al.* (2016) with a transgressive trend up to the upper part of FZ13 (Fig. 10).

As expected, Frasnian sections of SW Algeria display a similar sea-level evolution through middle and late Frasnian time as in neighbouring parts of Gondwana (Morocco). Differences in deposits (the absence or presence of the lower Kellwasser horizon), timing (changes in sea level occurring later in SW Algeria than elsewhere) and amplitude of changes in both litho- and biofacies between sites might result from the effects of locally different rates of tectonically driven subsidence. In addition, sampling bias cannot be excluded in highly condensed portions such as in the lower part of the Ben Zireg section or, on the contrary, when conodonts are rather scarce in deposits with high sedimentation rates, as occurs in the lower–middle Frasnian Marhouma trough (Mahboubi *et al.* 2015).

6. Conclusions

The investigated sections through the middle–upper Frasnian deposits are composed of seven marine lithofacies. These lithofacies are organized along a very low-angle, middle to outer ramp along the western part of the Saharian Platform. Condensed carbonate sedimentation occurred in the north (Ben Zireg), whereas abundant shaly deposits occur in the south (Marhouma). Vertical facies changes indicative of sea-level fluctuations are most perceptible at South Marhouma within the lower–middle and the upper Frasnian strata, where rapid shifts between deep and shallow lithofacies occur. During early–late Frasnian time, more stable conditions prevailed with the deposition of bioclastic mud- and wackestones. Conversely, at Ben Zireg these latter conditions characterize the condensed middle and lowermost-upper Frasnian succession. A deepening occurred in the upper part of FZ11, followed by a marked shallowing at the beginning of FZ12 and an average deepening up to the upper Kellwasser horizon. The latter is marked in both sections by a transgressive–regressive cycle.

Provisional measurements of magnetic susceptibility provided very low values. Shifts are more pronounced with rapid variations in the lower part of the middle Frasnian strata, remaining constantly rather low thereafter up to the Frasnian–Famennian boundary in both sections. In particular, no significant shift is observed at the equivalent levels of the Kellwasser deposits. More detailed and bed-by-bed measurements are necessary to consider MS trends comparatively.

A sea-level curve essentially built on the data acquired at Ben Zireg matches the standard curves already provided at a global scale. In particular, evidence of the middle Frasnian transgression, the lower FZ11 regression, the *semichatovae* transgression within FZ11, the lower FZ12 regression, the upper FZ13 transgression and the regression associated with the upper Kellwasser deposits are clearly observed in the Saharian Platform.

Acknowledgements. We are grateful to the Algerian authorities for providing permission to access the field. We thank Tadjedinne Hassen, Kada Abess and Brigitte Meyer-Berthaud for their help with fieldwork. We thank D. Pas, D. L. Boyer and two reviewers for suggesting improvements to the manuscript, and copy-editor Elaine Rowan. The first field trip was supported by the ANR Palasiafrica (ANR-08-JCJC-0017). A. Mahboubi is grateful to Jean-Louis Bodinier for his funding (IRSES MEDYNA grant) for one month. This is ISEM publication no. 2018-164.

References

Aigner T (1985) *Storm Depositional Systems: Dynamic Stratigraphy in Modern and Ancient Shallow-Marine Sequences*, Vol. **3**, Lecture Notes in Earth Sciences. Berlin: Springer-Verlag, 174 pp.

Alekseev AS, Kononova LI and Nikishin AM (1996) The Devonian and Carboniferous of the Moscow Syneclise (Russian platform): stratigraphy and sea-level changes. *Tectonophysics* **268**, 149–68.

Bambach RK, Knoll AH and Wang SC (2004) Origination, extinction, and mass depletions of marine diversity. *Paleobiology* **30**, 522–42.

Becker RT, Gradstein FM and Hammer O (2012) The Devonian period. In *The Geologic Time Scale 2012* (eds F Gradstein, J Ogg, M Schmitz and G Ogg), pp. 559–601. Amsterdam: Elsevier.

Belka Z and Wendt J (1992) Conodont biofacies pattern in the Kellwasser Facies (upper Frasnian/lower Fammenian) of the eastern Anti–Atlas, Morocco. *Palaeogeography, Palaeoclimatolology, Palaeoecology* **91**, 143–73.

Bendella M and Mehadji AO (2014) Depositional environment and ichnology (Nereites ichnofacies) of the Late Devonian Sahara region (SW Algeria). *Arabian Journal of Geology* **7**, 1–14.

Bohacs KM, Lazar OR and Demko TM (2014) Parasequence types in shelfal mudstone strata—Quantitative observations of lithofacies and stacking patterns and conceptual link to modern depositional regimes. *Geology* **42**, 131–4.

Bond D, Wignall PB and Racki G (2004) Extent and duration of marine anoxia during the Frasnian–Famennian (Late Devonian) mass extinction in Poland, Germany, Austria and France. *Geological Magazine* **141**, 173–93.

Bond DPG and Wignall P (2008) The role of sea-level change and marine anoxia in the Frasnian-Famennian (Late Devonian) mass extinction. *Palaeogeography, Palaeoclimatology, Palaeoecology* **263**, 107–18.

Boote DRD, Clark-Lowes DD and Traut MW (1998) Palaeozoic petroleum systems of North Africa. In *Petroleum Geology of North Africa* (eds DS Macgregor, RTJ Moody and DD Clark-Lowes), Vol. **132**, pp. 7–68. *Journal of the Geological Society of London*, Special Publication.

Boulvain F, Cornet P, Da Silva AC, Delaite G, Demany B, Humblet M, Renard M and Coen-Aubert M (2004) Reconstructing atoll-like mounds from the Frasnian of Belgium. *Facies* **50**, 313–26.

Boyer DL and Droser ML (2009) Palaeoecological patterns within the dysaerobic biofacies: examples from Devonian black shales of New York state. *Palaeogeography, Palaeoclimatology, Palaeoecology* **276**, 206–16.

Boyer DL, Owens JD, Lyons TW and Droser ML (2011) Joining forces: combined biological and geochemical proxies reveal a complex but refined high-resolution palaeo-oxygen history in Devonian epeiric seas. *Palaeogeography, Palaeoclimatology, Palaeoecology* **306**, 134–46.

Casier JC (2008) Résumés des communications et guide de l'excursion consacrée aux ostracodes du Dévonien Moyen et Supérieur de Dinant. In *22nd Réunions des Ostracologistes de Langue Française*, pp. 1–88. Bruxelles: Institut Royal des Sciences Naturelles de Belgique, Département de Paléontologie.

Chen D and Tucker ME (2003) Palaeokarst and its implication for the extinction event at the Frasnian–Famennian boundary (Guilin, south China). *Journal of the Geological Society of London* **161**, 895–8.

Cook HE, Mcdaniel PN, Mountjoy EW and Pray LC (1972) Allochthonous carbonate debris flows at Devonian bank ('reef') margins, Alberta, Canada. *Bulletin of Canadian Petroleum Geology* **20**, 439–97.

Crick RE, Ellwood BB, Hladil J, El Hassani A, Hrouda F and Chlupac I (2001) Magnetostratigraphy susceptibility of the Pridolian–Lochkovian (Silurian–Devonian) GSSP (Klonk, Czech Republic) and coeval sequence in Anti-Atlas Morocco. *Palaeogeography, Palaeoclimatololgy, Palaeoecology* **167**, 73–100.

Da Silva AC, De Vleeschouwer D, Boulvain F, Claeys P, Fagel N, Humblet M, Mabille C, Michel J, Sardar Abadi M, Pas D and Dekkers MJ (2013) Magnetic susceptibility as a high-resolution correlation tool and as a climatic proxy in Paleozoic rocks-merits and pitfalls: examples from the Devonian in Belgium. *Marine and Petroleum Geology* **46**, 173–89.

https://doi.org/10.1017/S0016756818000626 Published online by Cambridge University Press

Da Silva AC, Mabille C and Boulvain F (2009) Influence of sedimentary setting on the use of magnetic susceptibility: examples from the Devonian of Belgium. *Sedimentology* **56**, 1292–306.

Deb SP, Schieber J and Chaudhuri AK (2007) Microbial mat features, mudstones of the Mesoproterozoic Somanpalli Group, Pranhita-Godavari Basin, India. In *Atlas of Microbial Mat Features Preserved within the Siliciclastic Rock Record* (eds J Schieber, PK Bose, PG Eriksson, S Banerjee, SS Jadavpur, W Altermann and O Catuneanu), Vol. **2**, pp. 171–80. Amsterdam: Elsevier.

Donzeau M (1974) L'arc Anti-Atlas-Ougarta (Sahara Nord occidental, Algérie, Maroc). *Comptes Rendus de l'Académie des Sciences, Paris, (II)* **278**, 417–20.

Dopieralska J, Belka Z and Walczak A (2016) Nd isotope composition of conodonts: an accurate proxy of sea-level fluctuations. *Gondwana Research* **34**, 284–95.

Dunham RJ (1962) Classification of carbonate rocks according to depositional texture. In *Classification of Carbonate Rocks* (ed. WE Ham), pp. 108–21. Tulsa, Okla: American Association of Petroleum Geologists, Memoir no. 1.

Ellwood BB, Tomkin JH, El Hassani A, Bultynck P, Brett CE, Schindler E, Feist R and Bartholomew AJ (2011) A climate-driven model and development of a floating point time scale for the entire middle Devonian Givetian stage: a test using magnetostratigraphy susceptibility as a climate proxy. *Palaeogeography, Palaeoclimatololgy, Palaeoecology* **304**, 85–95.

Feist R, Mahboubi A and Girard C (2016) New Late Devonian phacopid trilobites from Marhouma, SW Algerian Sahara. *Bulletin of Geosciences* **91**, 243–59.

Filer JK (2002) Late Frasnian sedimentation cycles in the Appalachian basin–possible evidence for high frequency eustatic sea-level changes. *Sedimentary Geology* **154**, 31–52.

Flügel E (2004) *Microfacies of Carbonate Rocks: Analysis, Interpretation and Application*. New York: Springer-Verlag, Berlin, Heildelberg, 984 pp.

Folk RL (2005) Nannobacteria and the formation of framboidal pyrite: textural evidence. *Journal of Earth Systems in Sciences* **114**, 369–74.

Göddertz B (1987) Devonische Goniatiten aus SW-Algerien und ihre stratigraphische Einordnung in die Conodonten-Abfolge. *Palaeontographica Abtelung A* **197**, 127–220.

Hallam A and Wignall PB (1999) Mass extinctions and sea-level changes. *Earth Science Review* **48**, 217–50.

Haq BU and Schutter SR (2008) A chronology of Paleozoic sea-level changes. *Science* **322**, 64–8.

House MR and Ziegler W (eds) (1997) On sea-level fluctuations in the Devonian. *Courier Forschunginstitut Senckenberg* **199**, 1–146.

Hüneke H (2006) Erosion and deposition from bottom currents during the Givetian and Frasnian: response to intensified oceanic circulation between Gondwana and Laurussia. *Palaeogeography, Palaeoclimatology, Palaeoecology* **234**, 146–67.

Hüneke H (2013) Bioclastic contourites: depositional model for bottom-current redeposited pelagic carbonate ooze (Devonian, Moroccan Central Massif). *Zeitschriftder Deutschen Gesellschaft für Geowissenschaften* **164**, 253–77.

James NP and Choquette PW (1990) Limestone—the meteoric diagenetic environment. In *Diagenesis* (eds IA Mc Ilreath and DW Morrow), Vol. **4**, pp. 35–73. Geoscience Canada. Canada: Geological Association of Canada.

Johnson JG, Klapper G and Sandberg CA (1985) Devonian eustatic fluctuations in Euramerica. *Geological Society of America Bulletin* **96**, 567–87.

Johnson JG and Sandberg CA (1988) Devonian eustatic events in the Western United States and their biostratigraphic responses. In *Devonian of the World* (eds NJ McMillan, AF Embry and DJ Glass), Vol. **14**, pp. 171–8. Calgary: Canadian Petroleum Geology.

Kaźmierczak J, Kremer B and Racki G (2012) Late Devonian marine anoxia challenged by benthic cyanobacterial mats. *Geobiology* **10**, 371–83.

Klapper G and Barrick JE (1978) Conodont ecology: pelagic versus benthic. *Lethaia* **11**, 15–23.

Klapper G and Kirchgasser WT (2016) Frasnian Late Devonian conodont biostratigraphy in New York: graphic correlation and taxonomy. *Journal of Paleontology* **90**, 525–54.

Kremer B and Kaźmierczak J (2005) Cyanobacterial mats from Silurian black radiolarian cherts: phototrophic life at the edge of darkness? *Journal of Sedimentary Research* **75**, 897–906.

Lüning S, Wendt J, Belka Z and Kaufmann B (2004) Temporal–spatial reconstruction of the early Frasnian (Late Devonian) anoxia in NW Africa: new field data from the Ahnet Basin (Algeria). *Sedimentary Geology* **163**, 237–64.

MacLean LCW, Tyliszczak T, Gilbert PUPA, Zhou D, Pray TJ, Onstott TC and Southam G (2008) A high-resolution chemical and structural study of framboidal pyrite formed within a low-temperature bacterial biofilm. *Geobiology* **6**, 471–80.

Mahboubi A and Gatovsky Y (2014) Late Devonian conodonts and event stratigraphy in northwestern Algerian Sahara. *Journal of African Earth Sciences* **101**, 322–32.

Mahboubi A, Feist R, Cornée J-J, Mehadji AO and Girard C (2015) Frasnian (Late Devonian) conodonts and environment at the northern margin of the Algerian Sahara platform: the Ben Zireg section. *Geological Magazine* **152**, 844–57.

Mamet B and Préat A (2006) Iron-bacterial mediation in Phanerozoic red limestones: state of the art. *Sedimentary Geology* **185**, 147–57.

Morrow JR and Sandberg CA (2008) Evolution of Devonian carbonate-shelf margin, Nevada. *Geosphere* **4**, 445–58.

Mutti E, Lucchi FR, Seguret M and Zanzucchi G (1984) Seismoturbidites: a new group of resedimented deposits. *Marine Geology* **55**, 103–16.

Narkiewicz M (1988) Turning points in sedimentary development in the Late Devonian in southern Poland. In *Devonian of the World* (eds NJ McMillan, AF Embry and DJ Glass), Vol. **14**, pp. 619–36. Calgary: Canadian Petroleum Geology.

Pareyn C (1961) *Les Massifs Carbonifères du Sahara Sud-Oranais*. Paris: Publications du Centre de Recherches Sahariennes, série Géologie, 324 pp.

Pas D, Da Silva AC, Cornet P, Bultynck P, Königshof P and Boulvain F (2013) Sedimentary development of a continuous middle Devonian to Mississippian section from the fore-reef fringe of the Brilon reef complex (Rheinisches Schiefergebirge, Germany). *Facies* **59**, 969–90.

Pas D, Da Silva AC, Devleeschouwer X, Devleeschouwer D, Labaye C, Cornet P, Michel J and Boulvain F (2015) Sedimentary development and magnetic susceptibility evolution of the Frasnian in Western Belgium (Dinant Synclinorium, La Thure section). In *Magnetic Susceptibility Variation: a Window onto Ancient Environments and Climatic Variations* (eds AC Da Silva, MT Whalen, J Hladil, L Chadimova, D Chen, S Spassov, F Boulvain and X Devleeschouwer), pp. 15–36. Geological Society of London, Special Publication no. 414.

Pas D, Da Silva AC, Sutter T, Kido E, Bultynck P, Pondrelli M, Corradini C, Devleeschouwer X, Dojen C and Boulvain F (2014) Insight into the development of a carbonate platform through a multi-disciplinary approach: a case study from the Upper Devonian slope deposits of Mount Freikofel (Carnic Alps, Austria/Italy). *International Journal of Earth Sciences* **103**, 519–38.

Peckmann J and Thiel V (2004) Carbon cycling at ancient methane-seeps. *Chemical Geology* **205**, 443–67.

Petter G (1952) Dévonien moyen et supérieur. In *Les Chaines d'Ougarta et la Saoura* (eds HD Alimen, D Le Maitre, N Menchikoff, G Petter and A Poueyto), pp. 62–74. Alger: 19th Congrès Géologique International.

Petter G (1959) *Goniatites Dévoniennes du Sahara*. Alger: Service de la Carte Géologique de l'Algérie, 313 pp.

Pisarzowska A and Racki G (2012) Isotopic chemostratigraphy across the early-middle Frasnian transition (Late Devonian) on the south Polish carbonate shelf: a reference for the global punctata event. *Chemical Geology* **334**, 199–220.

Riquier L, Tribovillard N, Averbuch O, Joachimski MM, Racki G, Devleeschouwer X, El Albani A and Riboulleau A (2005) Productivity and bottom water redox conditions at the Frasnian-Famennian boundary on both sides of the Eovariscan belt: constraints from trace-element geochemistry. In *Understanding Late Devonian and Permian-Triassic Biotic and Climatic Events: Towards an Integrated Approach* (eds DJ Over, JR Morrow and PB Wignall), pp. 199–224. Developments in Palaeontology and Stratigraphy Series. Amsterdam: Elsevier.

Rossetti DF and Góes AM (2000) Deciphering the sedimentological imprint of paleoseismic events: an example from the Aptian Codó formation, northern Brazil. *Sedimentary Geology* **135**, 137–56.

https://doi.org/10.1017/S0016756818000626 Published online by Cambridge University Press

Sandberg CA (1976) Conodont biofacies of Late Devonian Polygnathus styriatus Zone in western United States. In *Conodont Paleoecology* (ed. CR Barnes), pp. 171–86. Montreal: Geological Association of Canada, Special Paper no. 15.

Sandberg CA, Morrow JR and Ziegler W (2002) Late Devonian sea-level changes, catastrophic events, and mass extinctions. *Special Papers of the Geological Society of America* **356**, 473–87.

Sandberg CA and Ziegler W (1979) Taxonomy and biofacies of important conodonts of Late Devonian styriacus Zone, United States and Germany. *Geology and Palaeontology* **13**, 173–212.

Sandberg CA, Ziegler W, Dreesen R and Butler JL (1992) Conodont biochronology, biofacies, taxonomy, and event stratigraphy around middle Frasnian Lion Mudmound (F2h), Frasnes, Belgium. *Courier Forschunginstitut Senckenberg* **150**, 1–87.

Schieber J (1986) The possible role of benthic microbial mats during the formation of carbonaceous shales in shallow Proterozoic basins. *Sedimentology* **33**, 521–36.

Schieber J (1989) Facies and origin of shales from the mid-proterozoic Newland formation, Belt basin, Montana, USA. *Sedimentology* **36**, 203–19.

Schieber J, Southard J and Thaisen K (2007) Accretion of mudstone beds from migrating floccule ripples. *Science* **318**, 1760–3.

Schülke I and Popp A (2005) Microfacies development, sea-level change, and conodont stratigraphy of Famennian mid- to deep platform deposits of the Beringhauser tunnel section (Rheinisches Schiefergebirge, Germany). *Facies* **50**, 647–64.

Seddon G and Sweet WC (1971) An ecologic model for conodonts. *Journal of Paleontology* **45**, 869–80.

Spalletta C and Vai GB (1984) Upper Devonian intraclast parabreccias interpreted as seismites. *Marine Geology* **55**, 133–44.

Stigall AL (2012) Speciation collapse and invasive species dynamics during the Late Devonian "mass extinction". *Geological Society of America, GSA Today* **22**, 4–9.

Sur S, Schieber J and Banerjee S (2006) Petrographic observations suggestive of microbial mats from Rampur Shale and Bijaigarh Shale, Vindhyan basin, India. *Journal of Earth System Science* **115**, 61–6.

Tian L, Tong J, Algeo TJ, Song H, Chu D, Shi L and Bottjer DJ (2014) Reconstruction of Early Triassic ocean redox conditions based on framboidal pyrite from the Nanpanjiang Basin, South China. *Palaeogeogeography, Palaeoclimatolology, Palaeoecology* **412**, 68–79.

Vierek A and Racki G (2011) Depositional versus ecological control on the conodont distribution in the Lower Frasnian fore-reef facies, Holy Cross Mountains, Poland. *Palaeogeography, Palaeoclimatology, Palaeoecology* **312**, 1–23.

Wendt J and Belka Z (1991) Age and depositional environment of Upper Devonian (early Frasnian to early Famennian) black shales and limestones (Kellwasser facies) in the eastern Anti-Atlas, Morocco. *Facies* **25**, 51–89.

Wendt J, Kaufmann B, Belka Z, Klug C and Lubeseder S (2006) Sedimentary evolution of a Palaeozoic basin and ridge system: the middle and Upper Devonian of the Ahnet and Mouydir (Algerian Sahara). *Geological Magazine* **143**, 269–99.

Weyant M (1988) Relationship between Devonian and Carboniferous strata near the northern confines of the Bechar basin, Algeria. *Courier Forschunginstitut Senckenberg* **100**, 235–41.

Whalen MT and Day JE (2010) Cross-basin variations in magnetic susceptibility influenced by changing sea level, paleogeography, and paleoclimate: Upper Devonian, Western Canada Sedimentary Basin. *Journal of Sedimentary Research* **80**, 1109–27.

Wignall PB, Newton R and Brookfield ME (2005) Pyrite framboid evidence for oxygen-poor deposition during the Permian–Triassic crisis in Kashmir. *Palaeogeography, Palaeoclimatology, Palaeoecology* **216**, 183–8.

Wright VP and Burchette TP (1996) Shallow-water carbonate environments. In *Sedimentary Environments: Processes, Facies, and Stratigraphy* (ed. HG Reading), pp. 325–94. Oxford: Blackwell Science.

https://doi.org/10.1017/S0016756818000626 Published online by Cambridge University Press